PAPER

Check for updates

Improving the ecological index in the solution processing of hybrid perovskites†

Niusha Heshmati, [ID] Niklas Almandinger, Thomas Fischer [ID] and Sanjay Mathur [ID] *

Lead halide perovskites are taking center stage among photoactive materials due to their highly tunable properties and potential applications in photovoltaics and light-emitting devices. Hybrid perovskites have demonstrated exceptionally high solar cell efficiencies, which have quickly approached those of silicon photovoltaics. However, their technological readiness is hindered by limited environmental stability, the use of toxic solvents such as N,N-dimethylformamide (DMF), and concerns over lead (Pb) toxicity. This research presents a new green solvent system that combines biodegradable dihydrolevoglucosenone (Cyrene™) and 2-methyltetrahydrofuran (2-MeTHF) as a sustainable alternative to the hazardous DMF. This eco-friendly solvent system reduces reliance on conventional aprotic solvents in perovskite solar cell processing. Additionally, ethyl acetate was employed as a green antisolvent in the one-step spin coating process to enhance crystallization, selected for its lower toxicity compared to other common solvents. Investigation of solvent–solute interactions by various characterization techniques led to an optimized solvent blend of Cy-THF : DMSO (70 : 30 vol%) with an added 7.5 vol% acetonitrile that resulted in a desirable viscosity and a stable perovskite precursor solution. Additives, including methylammonium chloride (MACl, CH_3NH_3Cl) and thiourea ($SC(NH_2)_2$), were incorporated to improve the crystallinity and surface coverage of the perovskite films. The resulting thin films of cubic perovskite exhibited enhanced film quality and superior stability under ambient conditions, with optoelectronic properties comparable to those of DMF-based perovskites, achieving 95% of the DMF-reference device's efficiency. These results demonstrate the promise of green solvent systems, derived from recyclable carbon, for sustainable perovskite processing.

Introduction

Lead halide perovskite solar cells were first discovered in 2009, with the initial devices achieving a modest power conversion efficiency (PCE) of 3.8%. Since then, extensive interdisciplinary research and consequent optimization of processing methods have propelled the PCE values to exceed 26% for single-junction configurations.[1,2] A key factor in the rise of perovskite research has been the easy accessibility to materials and their device integration, enabled by solution-based procedures, which are both cost-effective and highly reproducible.[3,4] Although solar energy is widely regarded as a promising clean energy source, a major barrier in the commercialization of perovskite solar cells relates to the toxicity of materials and solvents essential for their synthesis and processing.[5]

First, the use of lead (Pb) as an essential B site cation in the ABX_3 perovskite structure presents a significant environmental challenge. Efforts to substitute lead with elements from groups 14 and 15 of the periodic table have been explored; however, the PCE values in devices based on these alternative compositions fall short in competition with the lead-based PSCs.[6] To this end, research also focuses on the encapsulation of perovskite solar cells (PSCs) to ensure long-term stability and prevent lead leakage.[7,8] A second major environmental concern is the extensive use of organic solvents, particularly volatile and toxic solvents like N,N-dimethylformamide (DMF) that are inhibitive for ambient processing due to their potential health risks.[9] To emphasize the massive amount of required solvent, producing 1 GW of solar power with a blade-coated perovskite (15% module efficiency) demands about 3500 liters of solvent.[10] Although vapor phase deposition methods offer a solvent-free alternative, they require high vacuum equipment which increases costs, processing complexity, and energy demand. Particularly, for mixed-cation and mixed-anion perovskite compositions, achieving precise stoichiometry control remains a challenge mostly due to the different vapor pressure of each component.[11,12]

While significant efforts have been made to counteract lead toxicity in perovskite solar cells, comparatively less attention has been given to reducing the environmental impact by identifying green alternative solvents.[13,14] Recently, solvent

Department of Chemistry, Institute of Inorganic and Materials Chemistry, University of Cologne, Cologne, 50939, Germany. E-mail: sanjay.mathur@uni-koeln.de

28200 | *J. Mater. Chem. A*, 2025, **13**, 28200–28212

This journal is © The Royal Society of Chemistry 2025

Paper

engineering has received recognition as a potential strategy to develop solvent systems that are both high-performing and environmentally sustainable for PSC applications.[15] However, a key challenge in identifying green solvents capable of dissolving Pb halides (PbI$_2$, PbBr$_2$, and PbCl$_2$) is producing perovskite inks based on a single, stable solution suitable for the one-step spin coating method. As a result, green solvent research has primarily focused on simpler perovskite compositions (*e.g.* FAPbI$_3$, MAPbI$_3$).[16]

Besides DMF and dimethyl sulfoxide (DMSO), perovskite film depositions have been successfully conducted using other polar aprotic solvents (non-proton donating) such as γ-butyrolactone (GBL), *N*-methyl-2-pyrrolidone (NMP) and dimethylacetamide (DMAc).[17] The chemical appeal of polar aprotic solvents lies in their coordinative abilities to function as a Lewis-base and form adducts with metal species such as Pb^{2+} by donating electron pairs.[15,17,18] Recent reports have demonstrated that the polarity of these solvents significantly influences the coordination and stabilization of the lead-species in the solution.[19]

Oxygen (O) and nitrogen (N) are well-studied donor atoms, provided by solvents like γ-butyrolactone (C$_4$H$_6$O$_2$; GBL), *N*-methyl-2-pyrrolidone (C$_5$H$_9$NO; NMP), dimethylformamide (C$_3$H$_7$NO; DMF), dimethyl sulfoxide (C$_2$H$_6$OS; DMSO), acetonitrile (C$_2$H$_3$N; ACN), and water (H$_2$O). Solvent–solute analysis of perovskite solutions shows the predominance of $[PbI_x]^{2-x}$ iodoplumbate clusters, whose nuclearity is primarily determined by the coordination ability of the solvents used.[18] A common parameter to measure this coordination ability is Gutmann's donor number (DN), which correlates with the affinity of the solvent molecules to bind to Pb^{2+} species. To fabricate perovskite thin films with uniform grain sizes and defect-free structures needed for high-performance devices, it is crucial to achieve full dissolution of the ionic precursor salts. Also, simultaneously enabling the formation of high nuclearity clusters can reduce the perovskite's nucleation barrier by providing a high local concentration of precursor species. DMSO, with its strong oxygen donor capability, exhibits higher affinity for binding to Pb^{2+} compared to DMF, and that is evident in their respective donor numbers of 29.8 kcal mol^{-1} and 26.6 kcal mol^{-1}.[20,21] Typically, solvents with high donor numbers like DMSO compete with halide anions (I$^-$, Br$^-$, Cl$^-$) for coordination sites around Pb^{2+}, thus inhibiting the formation of halidoplumbates, and consequently forming stable precursor solutions. Conversely, solvents with lower donor numbers coordinate weakly to Pb^{2+} and promote halidoplumbate formation which is detrimental to obtaining phase-pure perovskites.[22] This highlights the importance of DMSO's contribution in forming higher nuclearity $[PbI_x]^{2-x}$ complexes with relatively low toxicity,[23] and the potential to create stable and eco-friendly solvent systems, while ensuring high-quality thin film formation.[17,18] Therefore, mixed-solvent systems are chemically engineered to modify and optimize solution characteristics such as polarity, viscosity, and solvent–solute interactions.[15] Volatile green solvents such as ethanol and acetonitrile represent a significant advancement in this research.[24]

However, their rapid nucleation rates may limit grain growth, which is essential for optimal device performance and stability.[25,26] On the other hand, the slower evaporation of aprotic solvents with controlled evaporation rates can result in larger grains with higher crystallinity, further improving the device performance.[27]

Dihydrolevoglucosenone (Cyrene™) derived from renewable and biodegradable cellulose is a green alternative for perovskite solar cell fabrication.[28,29] As an aprotic solvent, Cyrene minimizes the risk of proton-mediated degradation of perovskite films.[13] Given the presence of the carbonyl group, it can interact with lead ions to stabilize the precursor solution by forming intermediate complexes, similar to protic solvents.[30] However, Cyrene has a relatively high viscosity (14.5 cP compared to 0.92 cP for DMF, 1.65 cP for NMP, and 2.20 cP for DMSO) that can hinder the formation of perovskite inks with optimal rheology for various deposition techniques.[26,29] To counteract the coating challenges posed by high-viscosity solvents like Cyrene and achieve smooth film formation with full coverage, in this work solvent-blending is considered by developing solvent systems that retain the benefits of ecological solar cell processing while optimizing film properties.[29,31] A solvent-blend consisting of Cyrene and 2-methyltetrahydrofuran (2-MeTHF) in a ratio of 80 : 20 vol% (denoted as Cy-THF) was developed that significantly lowered the viscosity (3.72 cP) to become a promising alternative for high-volume hybrid perovskite ink production.

In this work, the mixed-solvent system combines the low-toxicity and ecological considerations of perovskite inks with enhanced film properties. Additionally, the optimized solvent blend enables a one-step perovskite film deposition with anti-solvent treatment. For making the entire process eco-friendly (Fig. 1), ethyl acetate (CH$_3$CO$_2$CH$_2$CH$_3$; EA) was used as a green antisolvent with a high threshold limit value and a lower boiling point (77 °C), compared to commonly used antisolvents like toluene (C$_6$H$_5$CH$_3$; TL) and chlorobenzene (C$_6$H$_5$Cl; CB).[32,33] Ultimately, the solar cells made using a green solvent achieve 95% of the performance of the DMF reference solar cells with 13.3% efficiency and higher stability.

Results and discussion

Solvent and solute interactions

The reported methods for manufacturing lead halide perovskite thin films commonly involve a solvent mixture of DMF : DMSO with 80 : 20 vol%.[34,35] This research aims to obtain a high-quality thin film processed from a sustainable green solvent-based solution centered around a Cyrene: 2-methyltetrahydrofuran (80 : 20 vol%) blend denoted as (Cy-THF). Fig. 2a shows 40 mg mL^{-1} perovskite precursor salts in Cy-THF. PbI$_2$ and PbBr$_2$ remain insoluble as yellow and white solids respectively resulting from the insufficient polarity and low hydrogen bonding affinity (δ_H) value of Cy-THF; therefore, co-solvent addition is necessary. DMSO was chosen as a co-solvent due to its low toxicity and the strong coordination effect on PbI$_2$ which was shown to be essential for full dissolution of the perovskite salts and formation of high-quality crystal phases.[34,36] FAI can be fully ionized in Cy-THF because of its low bonding energy
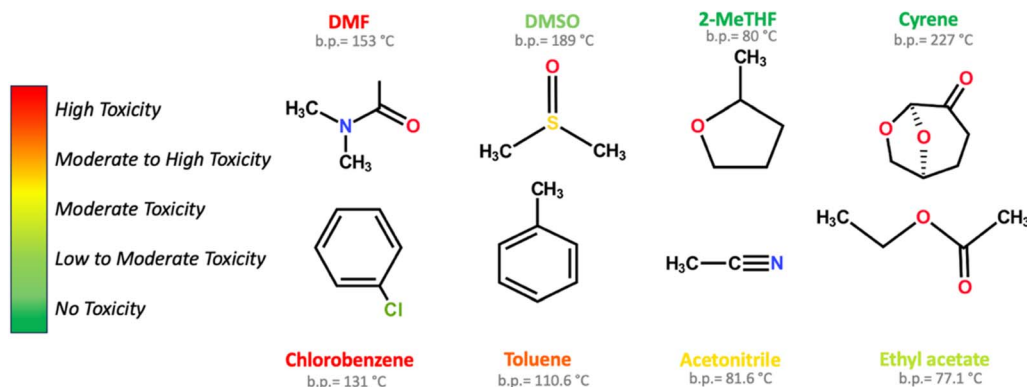
Fig. 1 Comparative analysis of organic solvents' structure and toxicity: identifying safer and less hazardous alternatives to main solvents (top row) and antisolvents (bottom row).

and results in a clear solution without DMSO. Experiments optimized the Cy-THF ratio, annealing conditions, and anti-solvent evaluation detailed in the ESI, Sections 2.1 and 2.2† for MAPbI$_3$ perovskite. Additionally, to gain a deeper under-standing of Cy-THF : DMSO solution properties, coordinating additives and suitability for perovskite precursor solutions, ^{1}H-NMR data of fresh and aged 1 M MAPbI$_3$ solutions are provided in ESI Section 2.3.† These results represent the suitability of the solvent mixture because of the major role that DMSO plays in coordinating PbI$_2$ to make the MAI-PbI$_2$-DMSO intermediate phase.[15] In view of the high stability reported for Cs$_{0.05}$(-MA$_{0.17}$FA$_{0.83}$)$_{0.95}$Pb(I$_{0.83}$Br$_{0.17}$)$_3$ perovskite (referred to as a triple-cation perovskite), within this research attempts were made to develop green solvents for triple cation perovskites.[37] In addition, 0.8 M concentration was chosen for the triple cation

perovskite to reduce the Pb amount and enhance solution stability.[38] The development of a green solvent-based triple cation perovskite with a single final ink formulation remains unexplored, and the complexity of the solution chemistry presents a significant challenge.[39]

As a starting point, the Cy-THF : DMSO : DMF (60 : 30 : 10 vol%) and DMF-free (70 : 30 : 0 vol%) solvent blends were evaluated to determine the possibility of complete DMF removal for the triple cation solution. The green solvent perovskite thin films were prepared by one-step spin coating onto FTO/mesoporous TiO$_2$ (m-TiO$_2$) and treated with EA as an anti-solvent, followed by annealing at 150 °C for 30 minutes. The degree of crystallinity was studied by X-ray diffraction (XRD) and Fig. 2b shows the XRD patterns. The measured signals show that the desired cubic lattice (100), (110), (111), (200), and (220)
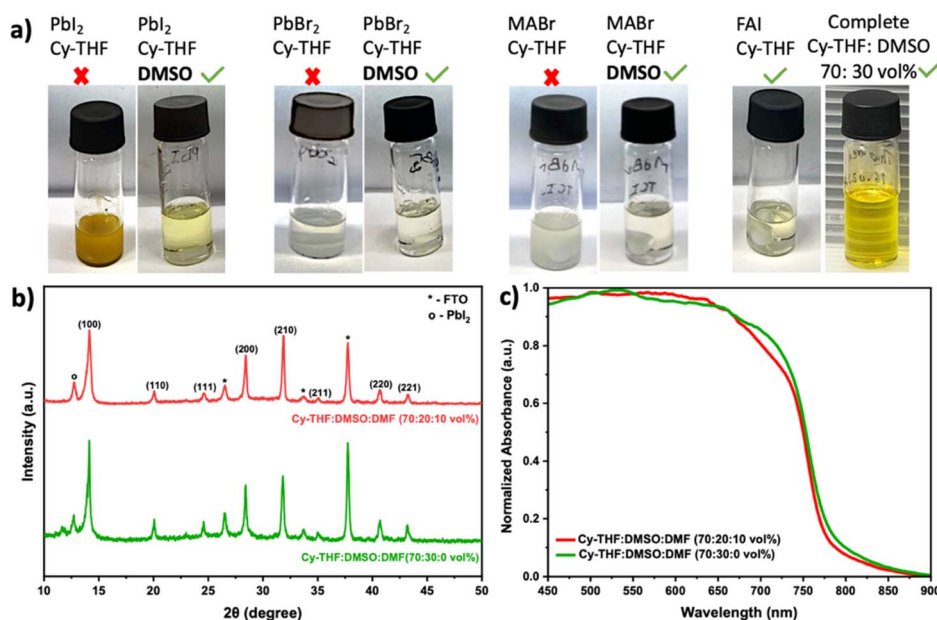

Fig. 2 (a) Solubility of PbI$_2$, PbBr$_2$, MABr, and FAI with 40 mg mL^{-1} concentration in Cy-THF and each component and full mixture in a solvent blend Cy-THF : DMSO (70 : 30 vol%). (b) Thin film XRD and (c) UV-Vis absorbance of perovskite thin films prepared on FTO/(m-TiO$_2$) from Cy-THF : DMSO : DMF (70 : 20 : 10 and 70 : 30 : 0 vol%) and 0.8 M triple cation precursors.

28202 | *J. Mater. Chem. A*, 2025, **13**, 28200–28212

This journal is © The Royal Society of Chemistry 2025

planes for the triple cation composition have been obtained for both thin films. Surprisingly, the full width at half maximum (FWHM) for all peaks especially (100) and (200) decreases for the DMF-free sample indicating higher crystallization.[40] Additionally, the presence of PbI_2 due to the incomplete formation of perovskite can significantly affect optoelectronic properties by increasing non-radiative charge carrier recombination and inducing surface defects, which is visible for both films' XRD patterns at $2\theta = 12.6°$.[41,42] To evaluate the photoabsorbance properties of perovskite thin films the UV-Vis spectra were measured and are shown in Fig. 2c. A clear absorption edge can be observed around a wavelength of 780 nm for both films that can be related to a bandgap energy of 1.59 eV, which agrees with the literature for the triple cation composition.[2] For the DMF-free thin film the absorbance spectrum is similar to that of the 10% DMF sample, and the absorption edge alone has a 5 nm red shift that can indicate the crystallinity enhancement for this sample, confirming the XRD results.[43] Although the removal of DMF has shown promising results and the addition of 30 vol% DMSO dissolves PbI_2 and forms a clear stable solution, the high viscosity of the Cy-THF : DMSO (70 : 30 vol%) solution remains a challenge that needs to be addressed.

Solvent engineering for perovskite inks

To adapt to the different coating methods, the precursor solution must confront issues such as viscosity, solution stability, and film wettability. To address the Cy-THF : DMSO (70 : 30 vol%) high viscosity challenge, the technique of "viscosity-blending" was employed which involves the incorporation of a new solvent with lower viscosity.[29] Acetonitrile (ACN) as a HSE recommended solvent,[6] with a very low viscosity of 0.38 cP at 25 °C, has gained attention for perovskite solar cell fabrication as an antisolvent, and also as an additive in the established DMF : DMSO solvent system.[44,45] It has been demonstrated that DMSO

with a high donor number of 29.8 kcal mol^{-1} as a main solvent and ACN with a low DN of 14.1 kcal mol^{-1} (ref. 21) as a cosolvent can significantly influence Pb^{2+} coordination and formation of high valence coordination spheres.[18] Perovskite precursor solutions were prepared with a foundation of Cy-THF : DMSO (70 : 30 vol%) and ACN was added in amounts of 5, 7.5, 10, and 12.5 vol% to the precursor solution over multiple experiments to investigate its influence on the applied solvent system.[17] The addition of ACN showed an immediate improvement for the solutions, and the viscosity significantly reduced and full dissolution of the perovskite salts were obtained after heating at 50 °C for only 30 minutes. In addition to high coordination by DMSO, the formation of Lewis acid-base pairs between ACN and PbI_2 enhanced the solubility of salts.[45] The precursor solutions showed rising film wettability, resulting in higher-quality thin films of cubic α perovskite.

Fig. 3a illustrates the XRD pattern, revealing the formation of a cubic α-phase with high crystallinity for films prepared with 7.5 and 10 vol% ACN addition. Peak intensities correlate with the microstructural change of the fabricated films, and intensity enhancement indicates preferred cubic lattice orientation improvement.[46] Addition of 7.5 vol% ACN leads to the reduction of PbI_2 hexagonal (marked peak at ~12.6°) which corresponds to the presence of intermediate phases such as $FAI-PbI_2-DMSO$/ Cyrene.[47] To study the film homogeneity, the samples were analyzed via scanning electron microscopy (SEM) presented in Fig. 3b. The SEM images for 7.5 vol% ACN show flake-shape grains resulting in incomplete surface coverage. Hence, utilization of acetonitrile in the perovskite precursor addresses several challenges, including viscosity, dissolution, and film wettability. Based on these results, the optimal amount of acetonitrile ranges between 7.5 and 10 vol% addition; however, full surface coverage and homogeneous film formation are still not achieved.
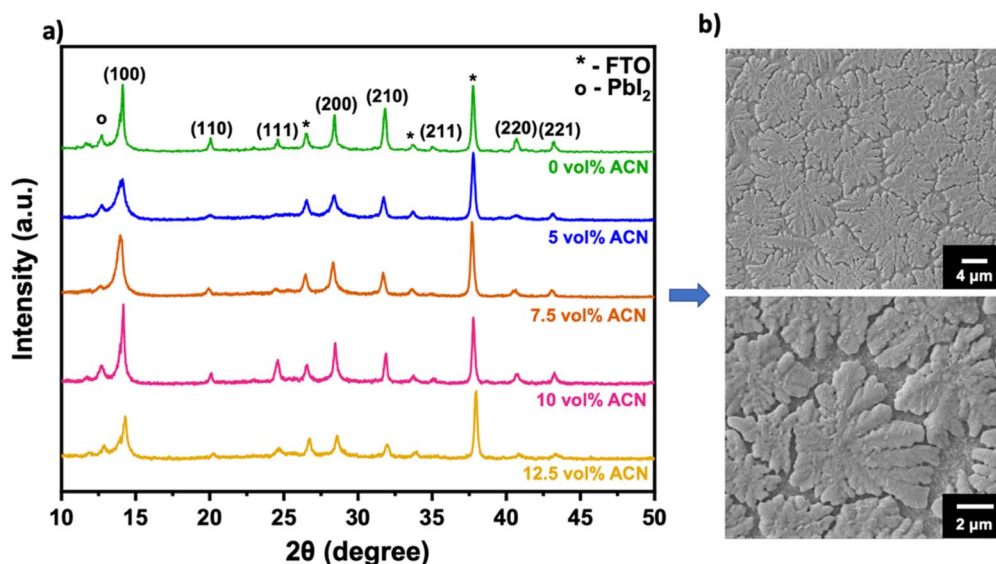

Fig. 3 (a) The XRD patterns of triple-cation perovskite thin films synthesized from different amounts of acetonitrile used as an additive to 1 mL Cy THF : DMSO (70 : 30 vol%) triple cation solution. (b) SEM images of a film prepared with addition of 7.5 vol% ACN to the precursor solution. Samples were prepared on FTO/mesoporous TiO_2.

This journal is © The Royal Society of Chemistry 2025

J. Mater. Chem. A, 2025, **13**, 28200–28212 | **28203**

Stabilization of perovskite by volatile salt addition

With the appropriate solvent and solute interactions established in a previous section the focus was on exploring additional treatments that directly influence the nucleation of the deposited perovskites. An approach that has garnered attention over recent years is the addition of volatile salt additives like methylammonium chloride (MACl) as a transitional stabilizer that preserves the crystal structure of a given perovskite while promoting the formation of stable, photoactive phases.[48,49] CH_3NH_3Cl will react with the perovskite precursor and form complexes like $PbI_2 \cdot CH_3NH_2$ and $PbI_2 \cdot HCl$ that lead to the gradual release of ions to control the nucleation and growth process, and CH_3NH_2 and HCl will evaporate during the annealing.[23] This approach has been geared towards the $FAPbI_3$ perovskite because of the common transition between the photoactive black perovskite α-phase and a photoinactive yellow δ-phase,[2,50,51] and addition of MACl resulted in pure α-phase crystallization. Given that the predominant component of the triple cation perovskite is FAI, this method could be an effective approach to enhance the film properties. The perovskite precursor solutions were prepared by adding MACl salt in amounts of 20% (wt% in relation to FAI) to the optimized solution of Cy-THF : DMSO (70 : 30) + 7.5–10 vol% of acetonitrile. The XRD measurements in Fig. 4a compared the effect of ACN amount and MACl addition on the crystallinity of thin films. Notably, XRD patterns of samples with MACl additive showed no detectable PbI_2, suggesting the absence of unreacted PbI_2 crystals, which can delay PSC degradation.[52] Moreover, the FWHM and intensity for the cubic perovskite planes have

drastically increased, and direct crystallization into the photo-active black perovskite α-phase films was achieved via MACl addition. The XRD peak at $2\theta \approx 36°$ corresponding to FTO substrate diffraction is considerably reduced in MACl treated films, which confirms the higher surface coverage. To shed light on this hypothesis the samples were analyzed via SEM, and Fig. 4b and c show considerable enhancement for grain shape and film coverage observed with 20 wt% MACl addition. However, the 10 vol% ACN-MACl film presented in Fig. 4b shows less homogeneity with more defects and pinholes in comparison to 7.5 vol% ACN (Fig. 4c). Therefore, this comparison clearly illustrates a notable enhancement in film crystallinity and growth associated with the addition of MACl. The grain size distribution for the optimized 7.5 vol% ACN and 20 wt% MACl film (Fig. 4c inset) ranges from 0.3 cm to 1.3 μm, with an average size of 0.8 μm. The grain size significantly influences the optoelectronic properties of polycrystalline lead halide perovskite films.[53] Accordingly, UV-Vis spectra and steady-state photoluminescence (PL) spectra are presented in Fig. 4d. The absorption spectra have a clear absorption edge at 767 nm corresponding to the calculated bandgap of ~1.61 eV, emphasizing the formation of a photoactive perovskite phase. The photoluminescence spectra also show a single and well-defined emission peak, showing high quality thin films with increased photoelectric properties.[54] The presence of a single emission peak near the absorption edge suggests the exclusive presence of perovskite in a single crystallographic phase, consistently observed in our XRD results.[55,56]
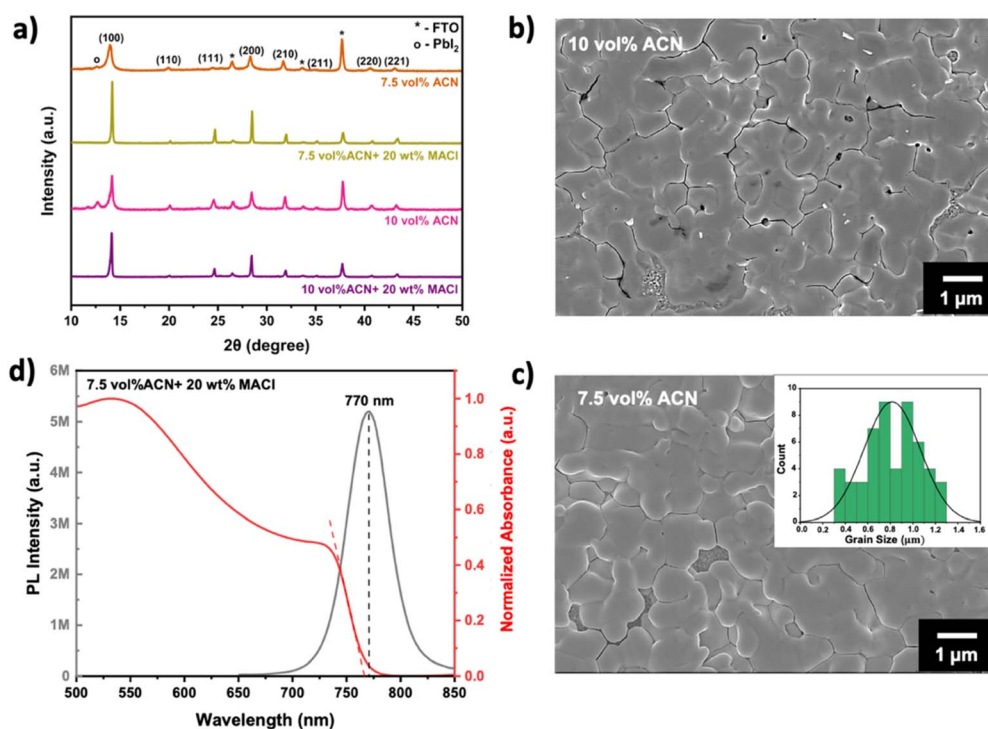

Fig. 4 (a) XRD patterns for the perovskite films containing 20 wt% MACl with 7.5 and 10 vol% ACN addition and comparison with MACl-free counterparts. SEM images of (b) 10 vol% ACN and 20 wt% MACl thin film, (c) 7.5 vol% ACN and 20 wt% MACl film, inset is the grain size distribution with a 0.82 μm average. (d) Normalized UV-Vis absorption and steady-state PL spectra of the optimized thin film.

28204 | J. Mater. Chem. A, 2025, 13, 28200–28212

This journal is © The Royal Society of Chemistry 2025

Control of the nucleation and growth of perovskite solar cells

Apart from altering the lead and organic precursors, the inclusion of certain ligand compounds, which act as electron donors (Lewis bases), can significantly influence the properties of perovskite films.[57] Thiourea ($SC(NH_2)_2$) as an organic compound has emerged as a promising candidate for enhancing grain size and improving film coverage when incorporated as an additive in a mixed halide perovskite solution. Incorporating thiourea ($SC(NH_2)_2$) as a Lewis base with a sulfur donor into the precursor solution is reported to control the perovskite phase evolution as well as nucleation and subsequent crystal growth processes.[58] The strong coordinating behavior of thiourea alters the solution and crystallization dynamics by increasing the Gibbs free energy, thereby reducing the number of nuclei formed.[59] Consequently, perovskite crystal growth initiates from fewer nucleation sites, leading to the development of larger grain sizes characterized by reduced grain boundary density.[60,61] Thiourea molecules containing CS and NH_2 functional groups exhibit dual roles: they coordinate with undercoordinated Pb^{2+} ions through Lewis acid–base interactions to mitigate defects and simultaneously establish hydrogen bonds with FA organic cations by forming the intermediate phase $FAI \cdot PbI_2 \cdot S{=}C(NH_2)_2$, thereby enhancing the stability of the perovskite framework.[62,63]

The use of sequential ethyl acetate (EA) antisolvent processing eliminated the remaining thiourea and enlarged the grain size.[63] Therefore, 20 wt% thiourea was added to the perovskite precursor, referred to as the "final green solvent" and compared with a reference DMF : DMSO solution.

Final solution evaluation

Implementation of a single-step spin coating process requires precise control over physical properties such as density, viscosity, and film wettability of the precursor solution.[64] Given the colloidal nature of the perovskite ink, dynamic light scattering (DLS) measurement was performed to investigate the size distribution of the particles in precursor solutions.[65] The DLS results in Fig. 5a show the particle size distribution to be centered between 0.8 and 2 nm for the reference ink. In contrast, the optimized green solution blend displays a broader colloidal size distribution, with particles centered around 2 to 9 nm. The larger average particle size correlates well with the higher viscosity observed in green solvent systems. In addition, the donor strengths of the solvents can influence the critical particle size to stabilize larger nuclei. The perovskite droplet
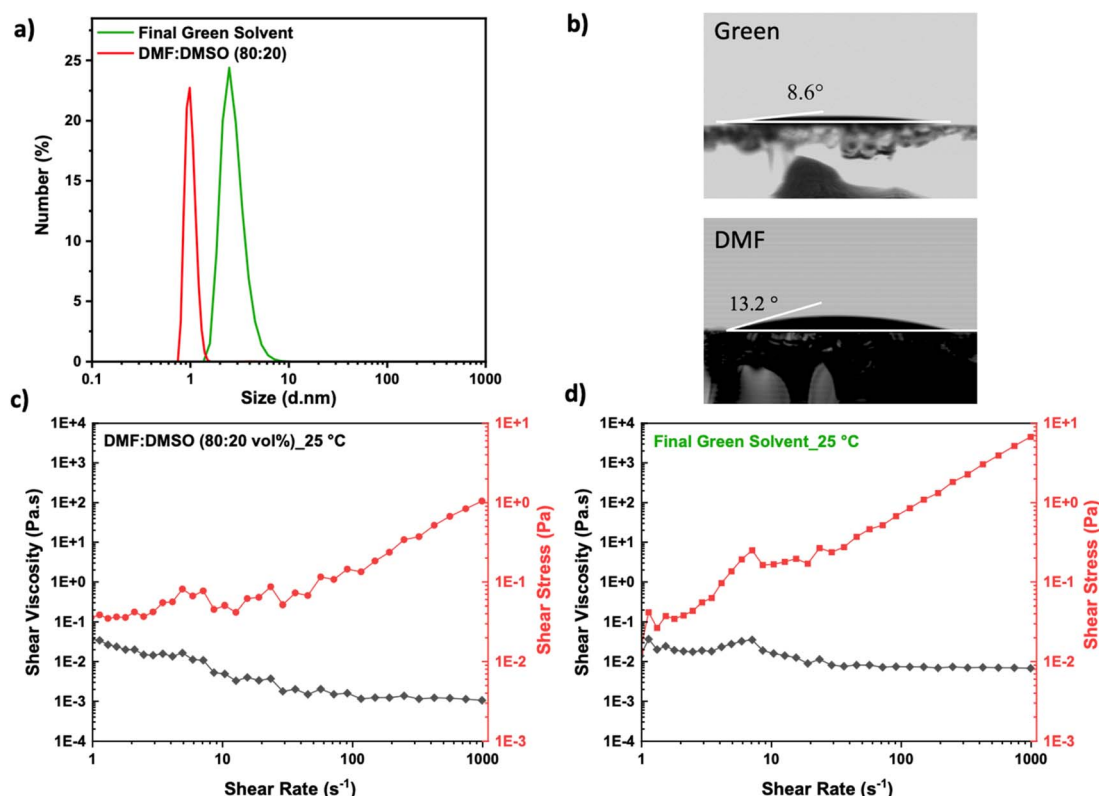

Fig. 5 (a) Comparison of the 0.8 M triple-cation lead halide perovskite solution in DMF : DMSO solvent and final green solvent analysed by DLS. (b) Contact angle of the 0.8 M triple-cation precursor ink on FTO/m-TiO$_2$ for the final green solvent, and DMF : DMSO reference sample. Both solutions have excellent wetting properties, with even lower than 10° achieved for the green solvent. Rheological characterization of perovskite precursor inks at 25 °C. (c) The reference ink formulated with DMF exhibits Newtonian behavior at higher shear rates, becoming shear-independent above ~100 s⁻¹. (d) The green solvent ink demonstrates Newtonian behavior starting from ~10 s⁻¹, suggesting improved viscosity characteristics and better processability under low-shear coating conditions. These differences highlight the potential of green solvent systems to offer superior coating performance and scalability for solution-based perovskite film deposition methods.

This journal is © The Royal Society of Chemistry 2025

J. Mater. Chem. A, 2025, **13**, 28200–28212 | **28205**

contact angle was measured on FTO/mesoporous-TiO_2 substrates, showing (Fig. 5b) improved wettability for the green solution blend droplet with a contact angle of 8.6°, while the DMF-reference solution droplet has a contact angle of 13.2°.[66]

A comparative evaluation of the rheological characteristics of perovskite inks in DMF : DMSO, acting as the reference solution, and the green solvent-based perovskite precursor (both at 0.8 M concentration) was performed at 25 °C. In high-shear regimes of ~1–1000 s^{-1}, the viscosity and flow behavior of perovskite precursor inks directly influence film formation, microstructural uniformity, and process scalability. It has been observed in previous reports that perovskite inks can exhibit either Newtonian or shear-thinning (pseudoplastic) behavior, depending on their composition, solvent system, and presence of additives.[64,67] Fig. 5c and d show that both solutions exhibit shear-thinning (pseudoplastic) behavior at low shear rates and transition to Newtonian behavior at higher shear rates.[68] Notably, the green ink exhibited a nearly constant viscosity (Newtonian behavior) around 10 s^{-1}, suggesting formation of stable perovskite precursor frameworks. This stable rheological profile across a wide shear range is advantageous for scalable, high-throughput coating methods, where predictable viscosity simplifies flow modeling and process control.[64,69] At 1 s^{-1}, the viscosities of the DMF : DMSO (34.0 cP) and green solvent (36.9 cP) inks are comparable, suggesting similar viscosity drag during early wetting stages. However, at 1000 s^{-1}, the DMF-reference ink shear thins to 1.06 cP, while the green solvent maintains a higher viscosity of 6.7 cP, indicating higher resistance to flow under dynamic coating conditions. This is manifested in more pronounced perovskite domains in green solvent processed films, which is expected to improve the charge transport properties due to the decreased grain boundary fraction, although enhancing the surface roughness.

Film coverage and grain size distribution

Considering the thiourea effect, the annealing temperature for thin films was chosen to start at 60 °C and ramped up to 150 °C over 30 minutes.[70] The low evaporation rate of the solvent helps to maintain the solution concentration close to the critical level for a long period. This results in a low concentration of nuclei, allowing the initially formed nuclei ample time and space to grow into large crystals.[71]

The surface of the final green optimized perovskite film was compared with that of the reference DMF : DMSO perovskite film using scanning electron microscopy (Fig. 6a and c). The surface morphologies demonstrate that the addition of 20 wt% thiourea to the green solvent resulted in a fully covered, defect-free perovskite surface. The grain size distribution (Fig. S6†) revealed a significant increase in crystal grain size for the green solvent system, with an average grain size exceeding 1.5 μm, which is more than six times higher than that of the DMF : DMSO film with a 225 nm average grain size. In addition, atomic force microscopy (AFM) analysis was employed to examine the surface morphology and roughness of the perovskite films. The results, presented in Fig. 6b and d, confirmed a progressive increase in grain size for the perovskite samples, consistent with the trends observed in SEM. Additionally, surface roughness increased in the same order, with root mean
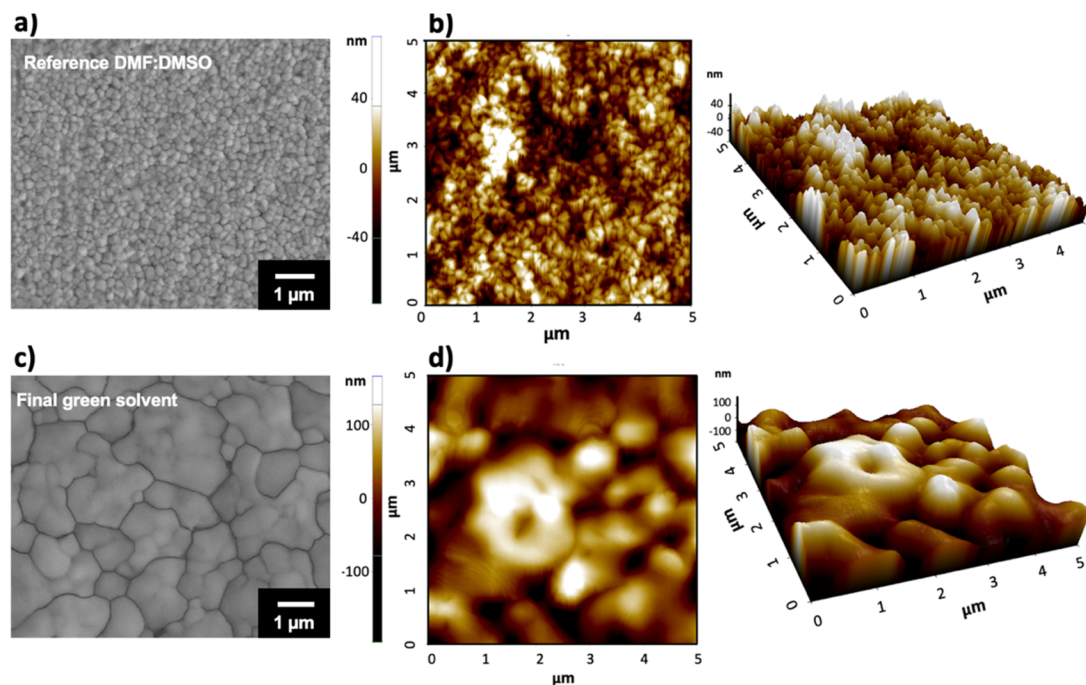

Fig. 6 (a) SEM image of the perovskite film fabricated using a DMF : DMSO solvent shows full coverage and small grains with an average size of 225 nm. (b) AFM topographic images showing an RMS roughness of 19.3 nm for DMF : DMSO processed thin films. (c) SEM image of the final perovskite film with 20 wt% thiourea in the green solvent and defect-free morphology with significant grain size increase with 1.65 μm. (d) AFM height and 3D topography images confirming higher surface roughness with RMS of 52.6 nm for the final green solvent.

28206 | J. Mater. Chem. A, 2025, 13, 28200–28212

This journal is © The Royal Society of Chemistry 2025

square (RMS) roughness values of 19.3 nm for the reference and 52.6 nm for the green solvent. This trend is further supported by 3D surface plot images, which clearly illustrate the gradual increase in surface roughness across the green solvent-based perovskite films. Increase of grain size has potential positive effects by reducing charge recombination due to fewer grain boundaries.[72] However, higher roughness may negatively impact the interface between the perovskite layer and the charge transport layers, potentially reducing charge extraction of the solar cells.

To verify the optoelectronic properties of the optimized perovskite light absorber film, UV-Vis and PL spectrophotometry were conducted and the corresponding spectra are shown in Fig. 7a. The characteristic absorbance onset observed at 782 nm for the green solvent and 790 nm for the reference film. A gradual increase in the absorbance up to 500 nm is clear for both films, while absorbance for the green ink is considerably higher than that of the reference film.[73] Besides, normalized PL results in a high emission peak for both samples with a narrower FWHM for the green solvent sample. To disclose the molecular interaction of the triple cation perovskite with green solvents and additives, Fourier transform infrared spectroscopy (FTIR) was performed on thin films and results are shown in Fig. 7b. Both films exhibit identical FTIR spectra, with absorption peaks observed at wavenumbers of 1350 cm^{-1} and 1477 cm^{-1}. These peaks are attributed to the vibrational modes of organic "–CH$_3$" groups present in the perovskite films. The corresponding absorption peaks of the amino groups in the perovskite films locate at the range of 1600–1750 cm^{-1} and 3200–3500 cm^{-1}.[74] Specifically, the N–H bending mode at 1468 cm^{-1} (symmetric) is observable, and selective monitoring of FA$^+$ and MA$^+$ is achieved through the measurement of the absorption associated with the C=N stretching mode of FA$^+$ (MA$^+$) at 1720 cm^{-1}, which corresponds to the symmetric bending of NH$_3$. Vibrations of N–H stretching of FA/MA indicate a dipole interaction with the components in solutions.[75,76]

The peak observed at 1617 cm^{-1} is attributed to the stretching of the carbonyl (C=O) bonds, which results from the effective coordination of DMF and Cy-THF solvent with the Lewis acid Pb^{2+}.[23] Additionally, the peak at 1020 cm^{-1}

corresponds to the S=O stretching associated with DMSO,[77] which contributes to the molecule's negative polarity.

The XRD results of the final green solvent thin film, compared with the reference films shown in Fig. 7c, demonstrate a significantly higher quality polycrystalline green perovskite thin film. The film exhibits a cubic phase with a (100) preferred orientation, consistent with previous studies highlighting the positive effects of thiourea addition on film crystallinity.[78]

Solar cell performance

As the final aim of this study, perovskite solar cells were fabricated using the optimized precursor system developed in this work (referred to as the green solvent) and compared with reference cells prepared using a DMF : DMSO solvent (referred to as the reference). The cells were assembled in a mesoscopic n–i–p structure: glass/FTO/mesoporous TiO$_2$/perovskite/Spiro-OMeTAD/Au, as shown in Fig. 8a. The cross-sectional SEM image illustrates a compact and homogeneous perovskite layer processed with the green solvent, exhibiting an approximate thickness of 500 nm.

The photovoltaic properties are presented in Fig. 8b, where the average performance of 28 cells measured for each category shows that green solvent perovskite cells exhibit behaviour almost identical to the reference sample. On average, the green solvent cells achieve 95% of the performance of the reference cells. However, the green solvent cells exhibit slightly lower averages for both J_{SC} and the fill factor. In perovskite solar cells, the interfaces between functional layers are critical for efficient carrier extraction and charge transport, as they directly impact device performance. Unwanted losses, such as those caused by interfacial recombination, can often lead to a reduction in J_{SC}, as noted in previous studies.[79,80] Our AFM results reveal higher surface roughness for the green solvent perovskite films, which likely contributes to the slightly reduced average performance. Increased roughness can create non-ideal interfaces, enhance recombination losses and hinder charge transport. Further evidence of these interfacial effects is shown in Fig. 8c, which illustrates the J–V curve of the champion cells. The green solvent cells display a slightly higher degree of hysteresis,
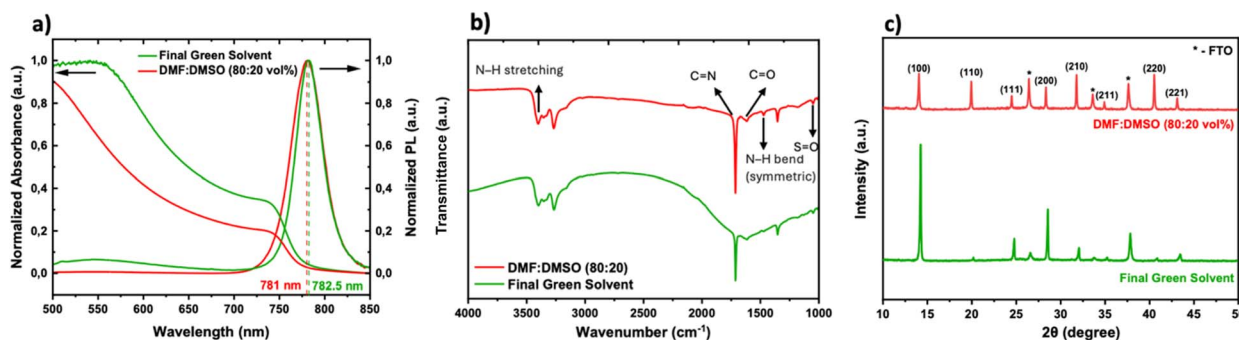

Fig. 7 Comparison of the final green solvent and reference DMF : DMSO perovskite thin films by (a) photoluminescence and UV-Vis absorbance spectra. (b) Fourier transform infrared spectroscopy of perovskite films which shows almost identical results for both films. (c) XRD pattern showing considerably higher crystallinity for the green solvent perovskite.
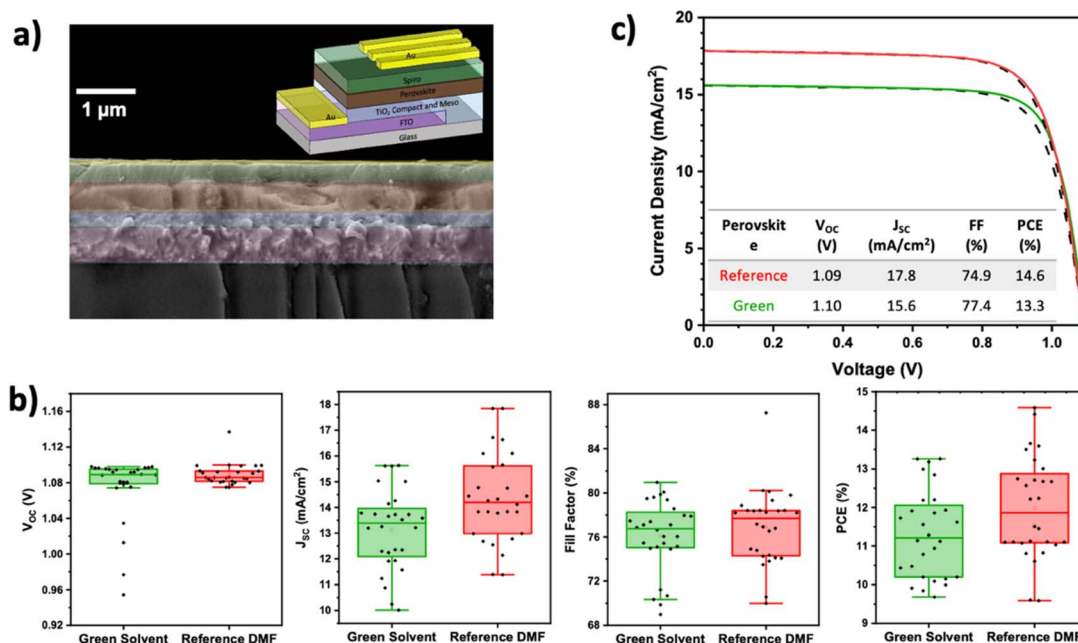
This journal is © The Royal Society of Chemistry 2025

J. Mater. Chem. A, 2025, **13**, 28200–28212 | **28207**

Fig. 8 (a) Schematic of the mesoscopic n−i−p structure perovskite solar cell. The electron transport material and hole transport material were TiO$_2$ and Spiro-OMeTAD respectively. (b) Box charts illustrating the statistical distribution of an open-circuit voltage (V_{OC}), short-circuit current density (J_{SC}), fill factor (FF) and power conversion efficiency (PCE) for green solvent and reference perovskite solar cells. (c) J−V curves obtained from reverse scans (solid line) and forward scans (dashed line) for champion cells.

a phenomenon that can be directly linked to the increased interfacial recombination.

Further research on surface modifications strategies could reduce surface roughness while maintaining large grain size, ensuring a well-defined interface between the perovskite and charge transport layers.[81,82] This could significantly enhance both device performance and stability beyond those of DMF-based solar cells.

Green solvent thin film stability

The deposited films were kept under extreme conditions with humidity ranging between 60% and 80%, ambient light, and 85 °C for two weeks. Fig. 9a shows images from the reference and final green solvent samples during this period. The degradation of the reference perovskite film is evident by its color change from black to yellow (characteristic of PbI$_2$) after six days. In contrast, the green solvent thin film shows less color variation, indicating greater thermal and moisture stability.[83]

This is further confirmed by XRD analysis on day seven, as shown in Fig. 9b. The reference sample almost completely lost its perovskite-related peaks, with intensified PbI$_2$ trigonal $P\bar{3}m1$ peaks appearing.[84] Although the green solvent film also underwent some degradation to PbI$_2$, its perovskite peaks remain fully detectable. To explain this difference first the solution stability can be considered. DMF-based perovskites readily undergo hydrolysis at room temperature when coordinated with a metal center (like Pb^{2+}) and break down into formic acid (HCOOH) and dimethylamine ((CH$_3$)$_2$NH) (DMA).[85] DMA is a stronger Lewis base compared to DMF or DMSO, and it

forms stable complexes with Lewis acids such as Pb^{2+}, Cs$^+$, and PbX$^+$. Formate ions have stronger bidentate ligand interactions with Cs$^+$ and Pb^{2+} than halides and displace halide ions (X$^-$) from PbX$_2$, forming Pb(HCOO)$_2$, which affects the overall stability of the solution. Thus, the equilibrium of precursor solution complexes is influenced by DMA$^+$ and formate (HCOO$^-$) and reduces solution stability.[86] Secondly, the degradation rate depends on grain size; smaller grains increase boundaries, accelerating perovskite degradation in humid environments.[87] Therefore, green solvent films, with larger grain sizes (hundreds of nm to micrometers), offer greater stability than DMF films. In addition, enhancing crystal quality improves longevity,[88] and our research confirms that improved crystallinity, especially in the (100) facet, enhances green solvent film stability.

To investigate the impact of the green solvent system on device stability, the solar cells presented in Fig. 8 were remeasured for PCE, after storing them for five months in a nitrogen-filled glovebox. As shown in Fig. 9c–e the highest and the average PCE of the green solvent-based devices remained marginally higher than those of the DMF-based reference, suggesting a modest stability benefit. However, a more pronounced hysteresis was observed in the green solvent devices after aging, indicating possible ion migration or interfacial instability. This may be attributed to the higher perovskite surface roughness and increased solution viscosity, which can lead to the formation of pinholes and voids in perovskite films.[89] In addition, both devices exhibited a reduction in PCE mostly due to the considerable loss of fill factor, possibly attributed to (i) the diffusion of gold from the top electrode that
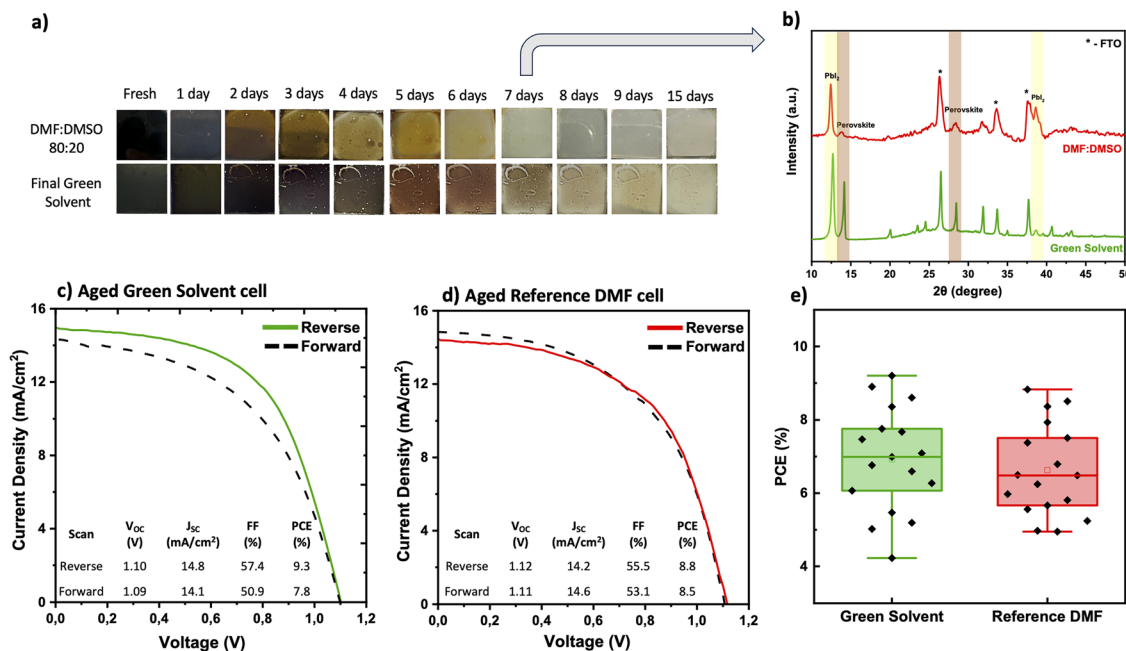
28208 | *J. Mater. Chem. A*, 2025, **13**, 28200–28212

This journal is © The Royal Society of Chemistry 2025

Fig. 9 (a) Photographs of the triple cation perovskite at ambient light, relative humidity of 60–80% and 85 °C heating. (b) XRD patterns of perovskite films on day seven of the stability test showing PbI_2 formation for both samples, and complete vanishing of perovskite peaks for the reference DMF : DMSO film. Samples stored in a nitrogen-filled glovebox for five months and $J–V$ curves obtained from reverse and forward scans for (c) the green solvent champion cell and (d) DMF-reference champion cell. (e) Box charts illustrating the statistical distribution of power conversion efficiency (PCE) for the green solvent and reference perovskite solar cells show a higher average for green solvent cells.

can penetrate the perovskite or transport layers to introduce recombination sites and increase series resistance (observed here),[90] and (ii) degradation of the hole transport layer, where Spiro-OMeTAD is known to suffer from dopant loss or oxidation state changes over time, even under inert conditions.[50]

Conclusions

This work demonstrates the potential of green solvent systems in efficient processing of high-performance triple cation perovskite $Cs_{0.05}(MA_{0.17}FA_{0.83})_{0.95}Pb(I_{0.83}Br_{0.17})_3$. Our optimized 70 : 30 vol% Cy-THF : DMSO solvent mixture produces a fully dissolved precursor solution, while the addition of acetonitrile (7.5 vol%) with a donor number of 14.1 kcal mol^{-1} and a low viscosity of 0.38 cP effectively reduces the overall viscosity of the solution. Addition of 20 wt% methylammonium chloride (MACl, CH_3NH_3Cl) and thiourea ($SC(NH_2)_2$) regulates ion release leading to the formation of a fully covered thin film with enhanced grain size. Notably, all solvents and additives were combined into a single solution, and the clear resulting ink is ready after less than one hour of stirring at 50 °C. This represents a significant achievement in simplifying the fabrication process for multi-cation perovskites, enabling the use of a single ink with a green solvent system. Additionally, the use of a lower solution molarity (0.8 M) reduces lead consumption. Finally, the ecological index of our approach was further increased by replacing commonly used anti-solvents with ethyl acetate (EA). Therefore, in this work, we successfully eliminated DMF from the solvent system by using 70% cellulose base solvent blend

Cyrene_2-MeTHF and 30% DMSO to fully dissolve the perovskite precursor. These additives facilitated the direct formation of a highly crystalline, photoactive cubic-phase perovskite with excellent optoelectronic properties. Achieving 95% of the performance of the DMF-based reference perovskite with a fully green solvent and antisolvent triple-cation solar cell is a significant highlight of this work. This demonstrates the potential of green solvent approaches to deliver high-efficiency perovskite solar cells while promoting more sustainable and environmentally friendly fabrication processes.

Data availability

The data supporting this article have been included as part of the ESI.†

Author contributions

Niusha Heshmati: conceptualization, data curation, formal analysis, investigation, methodology, validation, visualization, writing – original draft, writing – review & editing. Niklas Almandinger: investigation, formal analysis, visualization. Thomas Fischer: methodology. Sanjay Mathur: funding acquisition, project administration, resources, supervision, writing – review & editing.

Conflicts of interest

The authors declare no conflicts of interest.

This journal is © The Royal Society of Chemistry 2025

J. Mater. Chem. A, 2025, **13**, 28200–28212 | **28209**

Acknowledgements

Notes and references

1 A. Kojima, K. Teshima, Y. Shirai and T. Miyasaka, *J. Am. Chem. Soc.*, 2009, **131**, 6050.

2 F. Ünlü, E. Jung, J. Haddad, A. Kulkarni, S. Öz, H. Choi, T. Fischer, S. Chakraborty, T. Kirchartz and S. Mathur, *APL Mater.*, 2020, **8**(7), 070901.

3 D. Zhou, T. Zhou, Y. Tian, X. Zhu and Y. Tu, *J. Nanomater.*, 2018, **2018**, 1.

4 M. Cherasse, N. Heshmati, J. M. Urban, F. Ünlü, M. S. Spencer, M. Frenzel, L. Perfetti, S. Mathur and S. F. Maehrlein, *Small*, 2025, **21**, 2500977.

5 L. Schmidt-Mende, V. Dyakonov, S. Olthof, F. Ünlü, K. M. T. Lê, S. Mathur, A. D. Karabanov, D. C. Lupascu, L. M. Herz, A. Hinderhofer, F. Schreiber, A. Chernikov, D. A. Egger, O. Shargaieva, C. Cocchi, E. Unger, M. Saliba, M. M. Byranvand, M. Kroll, F. Nehm, K. Leo, A. Redinger, J. Höcker, T. Kirchartz, J. Warby, E. Gutierrez-Partida, D. Neher, M. Stolterfoht, U. Würfel, M. Unmüssig, J. Herterich, C. Baretzky, J. Mohanraj, M. Thelakkat, C. Maheu, W. Jaegermann, T. Mayer, J. Rieger, T. Fauster, D. Niesner, F. Yang, S. Albrecht, T. Riedl, A. Fakharuddin, M. Vasilopoulou, Y. Vaynzof, D. Moia, J. Maier, M. Franckevičius, V. Gulbinas, R. A. Kerner, L. Zhao, B. P. Rand, N. Glück, T. Bein, F. Matteocci, L. A. Castriotta, A. Di Carlo, M. Scheffler and C. Draxl, *APL Mater.*, 2021, **9**(10), 109202.

6 S. K. Podapangi, F. Jafarzadeh, S. Mattiello, T. B. Korukonda, A. Singh, L. Beverina and T. M. Brown, *Green Solvents, Materials, and Lead-free Semiconductors for Sustainable Fabrication of Perovskite Solar Cells*, Royal Society of Chemistry, 2023, vol. 13, pp. 18165–18206.

7 M. Ren, X. Qian, Y. Chen, T. Wang and Y. Zhao, *J. Hazard. Mater.*, 2022, **426**, 127848.

8 Y. Jiang, L. Qiu, E. J. Juarez-Perez, L. K. Ono, Z. Hu, Z. Liu, Z. Wu, L. Meng, Q. Wang and Y. Qi, *Nat. Energy*, 2019, **4**, 585.

9 X. Wu, D. Zhang, X. Wang, X. Jiang, B. Liu, B. Li, Z. Li, D. Gao, C. Zhang, Y. Wang and Z. Zhu, *Eco-friendly Perovskite Solar Cells: from Materials Design to Device Processing and Recycling*, John Wiley and Sons Inc, 2023, Vol. 5.

10 N.-G. Park, *Nat. Sustain.*, 2020, **4**, 192.

11 H. Hu, M. Singh, X. Wan, J. Tang, C.-W. Chu and G. Li, *J. Mater. Chem. A*, 2020, **8**, 1578.

12 F. U. Kosasih, E. Erdenebileg, N. Mathews, S. G. Mhaisalkar and A. Bruno, *Joule*, 2022, **6**, 2692.

13 J. Han, R. H. Kim, S. Huang, J. Kim and J. S. Yun, *Sol. RRL*, 2024, **8**, 2400262.

14 H.-S. Kim, Y.-J. An, J. Il Kwak, H. J. Kim, H. S. Jung and N.-G. Park, *ACS Energy Lett.*, 2022, **7**, 1154.

15 J. Jiao, C. Yang, Z. Wang, C. Yan and C. Fang, *Results Eng.*, 2023, **18**, 101158.

16 H. J. Kim, Y. J. Kim, G. S. Han and H. S. Jung, *Sol. RRL*, 2024, **8**(5), 2300910.

17 A. J. Doolin, R. G. Charles, C. S. P. De Castro, R. G. Rodriguez, E. V. Péan, R. Patidar, T. Dunlop, C. Charbonneau, T. Watson and M. L. Davies, *Green Chem.*, 2021, **23**, 2471.

18 E. Radicchi, E. Mosconi, F. Elisei, F. Nunzi and F. De Angelis, *ACS Appl. Energy Mater.*, 2019, **2**, 3400.

19 F. Ünlü, *Green inks and Lead-free Compositions in Perovskite and Allied Materials for Photovoltaic Applications*, Doctoral thesis, Dr. Hut, 2022.

20 V. Gutmann, *Coord. Chem. Rev.*, 1976, **18**, 225.

21 R. Stenutz, Gutmann acceptor and donor number, Stenutz, 2023, http://www.stenutz.eu/chem/solv21.php.

22 J. C. Hamill, J. Schwartz and Y.-L. Loo, *ACS Energy Lett.*, 2018, **3**, 92.

23 H.-S. Yun, H. W. Kwon, M. J. Paik, S. Hong, J. Kim, E. Noh, J. Park, Y. Lee and S. Il Seok, *Nat. Energy*, 2022, **7**, 828.

24 N. K. Noel, S. N. Habisreutinger, B. Wenger, M. T. Klug, M. T. Hörantner, M. B. Johnston, R. J. Nicholas, D. T. Moore and H. J. Snaith, *Energy Environ. Sci.*, 2017, **10**, 145.

25 D. Zheng, F. Raffin, P. Volovitch and T. Pauporté, *Nat. Commun.*, 2022, **13**, 6655.

26 L. Chao, T. Niu, W. Gao, C. Ran, L. Song, Y. Chen and W. Huang, *Adv. Mater.*, 2021, **33**(14), 2005410.

27 X. Cao, L. Zhi, Y. Jia, Y. Li, K. Zhao, X. Cui, L. Ci, D. Zhuang and J. Wei, *ACS Appl. Mater. Interfaces*, 2019, **11**, 7639.

28 D. Kong and A. V. Dolzhenko, *Sustain. Chem. Pharm.*, 2022, **25**, 100591.

29 C. Sullivan, Y. Zhang, G. Xu, L. Christianson, F. Luengo, T. Halkoski and P. Gao, *Green Chem.*, 2022, **24**, 7184.

30 Y. Zhong, Z. Liu, X. Luo, G. Liu, X. Wang, J. He, W. Sheng, D. Yu, C. Liang, L. Tan and Y. Chen, *Energy Environ. Sci.*, 2024, **17**, 5500.

31 G. S. Shin, J. Kim, S. Lee and N. Park, *Bull. Korean Chem. Soc.*, 2021, **42**, 1112.

32 L. Xu, S. Che, J. Huang, D. Xie, Y. Yao, P. Wang, P. Lin, H. Piao, H. Hu, C. Cui, F. Wu, D. Yang and X. Yu, *Appl. Phys. Lett.*, 2019, **115**(3), 033101.

33 Q. Chen, J. C.-R. Ke, D. Wang, M. Z. Mokhtar, A. G. Thomas and Z. Liu, *Appl. Surf. Sci.*, 2021, **536**, 147949.

34 Y. Rong, Z. Tang, Y. Zhao, X. Zhong, S. Venkatesan, H. Graham, M. Patton, Y. Jing, A. M. Guloy and Y. Yao, *Nanoscale*, 2015, **7**, 10595.

35 A. A. Petrov, A. A. Ordinartsev, S. A. Fateev, E. A. Goodilin and A. B. Tarasov, *Molecules*, 2021, **26**(24), 7541.

28210 | *J. Mater. Chem. A*, 2025, **13**, 28200–28212

This journal is © The Royal Society of Chemistry 2025

36 N. J. Jeon, J. H. Noh, Y. C. Kim, W. S. Yang, S. Ryu and S. Il Seok, *Nat. Mater.*, 2014, **13**, 897.

37 N. Jaiswal, V. P. Singh, D. Kumari and S. K. Pandey, *Energy Technol.*, 2024, **12**(2), 2300639.

38 D. A. Chalkias, A. Mourtzikou, G. Katsagounos, A. N. Kalarakis and E. Stathatos, *Small Methods*, 2023, **7**(10), 2300664.

39 J. Küffner, J. Hanisch, T. Wahl, J. Zillner, E. Ahlswede and M. Powalla, *ACS Appl. Energy Mater.*, 2021, **4**, 11700.

40 S. Lin, S. Wu, D. Guo, H. Huang, X. Zhou, D. Zhang, K. Zhou, W. Zhang, Y. Hu, Y. Gao and C. Zhou, *Small Methods*, 2023, **7**(4), 2201663.

41 Z. Ahmad, R. A. Scheidt, M. P. Hautzinger, K. Zhu, M. C. Beard and G. Galli, *ACS Energy Lett.*, 2022, **7**, 1912.

42 F. Ren, H. Xiang, K. Zhao and C. Liu, *J. Mater. Chem. C*, 2023, **11**, 13281.

43 S. M. Jain, B. Philippe, E. M. J. Johansson, B. Park, H. Rensmo, T. Edvinsson and G. Boschloo, *J. Mater. Chem. A*, 2016, **4**, 2630.

44 H. Li, Y. Xia, C. Wang, G. Wang, Y. Chen, L. Guo, D. Luo and S. Wen, *ACS Appl. Mater. Interfaces*, 2019, **11**, 34989.

45 Y. Yang, J. Wu, T. Wu, Z. Xu, X. Liu, Q. Guo and X. He, *J. Colloid Interface Sci.*, 2018, **531**, 602.

46 F. Zhao, J. Zhong, L. Zhang, P. Yong, J. Lu, M. Xu, Y. Cheng and Z. Ku, *Sol. RRL*, 2023, **7**(11), 2300062.

47 W. Xiang, J. Zhang, S. Liu, S. Albrecht, A. Hagfeldt and Z. Wang, *Joule*, 2022, **6**, 315.

48 C. Mu, J. Pan, S. Feng, Q. Li and D. Xu, *Adv. Energy Mater.*, 2017, **7**(6), 1601297.

49 M. Kim, G. H. Kim, T. K. Lee, I. W. Choi, H. W. Choi, Y. Jo, Y. J. Yoon, J. W. Kim, J. Lee, D. Huh, H. Lee, S. K. Kwak, J. Y. Kim and D. S. Kim, *Joule*, 2019, **3**, 2179.

50 M. Saliba, T. Matsui, J. Y. Seo, K. Domanski, J. P. Correa-Baena, M. K. Nazeeruddin, S. M. Zakeeruddin, W. Tress, A. Abate, A. Hagfeldt and M. Grätzel, *Energy Environ. Sci.*, 2016, **9**, 1989.

51 B. J. Kim, H. Choi, S. Park, M. B. Johansson, G. Boschloo and M. Kim, *ACS Sustain. Chem. Eng.*, 2024, **12**, 13371.

52 G. Tumen-Ulzii, C. Qin, D. Klotz, M. R. Leyden, P. Wang, M. Auffray, T. Fujihara, T. Matsushima, J. Lee, S. Lee, Y. Yang and C. Adachi, *Adv. Mater.*, 2020, **32**, 1905035.

53 C. Stavrakas, S. J. Zelewski, K. Frohna, E. P. Booker, K. Galkowski, K. Ji, E. Ruggeri, S. Mackowski, R. Kudrawiec, P. Plochocka and S. D. Stranks, *Adv. Energy Mater.*, 2019, **9**, 1901883.

54 T. P. A. van der Pol, K. Datta, M. M. Wienk and R. A. J. Janssen, *Adv. Opt. Mater.*, 2022, **10**, 2102557.

55 N. Heshmati, M. R. Mohammadi, P. Abachi and S. O. Martinez-Chapa, *New J. Chem.*, 2021, **45**, 788.

56 S. Jeong, H. C. Yoon, N. S. Han, J. H. Oh, S. M. Park, B. K. Min, Y. R. Do and J. K. Song, *J. Phys. Chem. C*, 2017, **121**, 3149.

57 S. Wang, Z. Ma, B. Liu, W. Wu, Y. Zhu, R. Ma and C. Wang, *Sol. RRL*, 2018, **2**, 1800034.

58 Y. Li, Y. Duan, J. Feng, Y. Sun, K. Wang, H. Li, H. Wang, Z. Zang, H. Zhou, D. Xu, M. Wu, Y. Li, Z. Xie, Z. Liu, J. Huang, Y. Yao, Q. Peng, Q. Fan, N. Yuan, J. Ding, S. Liu and Z. Liu, *Angew. Chem., Int. Ed.*, 2024, **63**, 202410378.

59 K. Lê, N. Heshmati and S. Mathur, *Nano Convergence*, 2023, **10**, 47.

60 J. V. Patil, S. S. Mali and C. K. Hong, *Nanoscale*, 2019, **11**, 21824.

61 X. Yang, H. Xiang, J. Huang, C. Zhou, R. Ran, W. Wang, W. Zhou and Z. Shao, *J. Colloid Interface Sci.*, 2022, **628**, 476.

62 Q. Sun, B. Tuo, Z. Ren, T. Xue, Y. Zhang, J. Ma, P. Li and Y. Song, *Adv. Funct. Mater.*, 2022, **32**(51), 220885.

63 C. Fei, B. Li, R. Zhang, H. Fu, J. Tian and G. Cao, *Adv. Energy Mater.*, 2017, **7**(9), 1602017.

64 M.-R. Ahmadian-Yazdi, A. Rahimzadeh, Z. Chouqi, Y. Miao and M. Eslamian, *AIP Adv.*, 2018, **8**(2), 025109.

65 P. Boonmongkolras, D. Kim, E. M. Alhabshi, I. Gereige and B. Shin, *RSC Adv.*, 2018, **8**, 21551.

66 Y. Miao, M. Ren, Y. Chen, H. Wang, H. Chen, X. Liu, T. Wang and Y. Zhao, *Nat. Sustain.*, 2023, **6**, 1465.

67 F. Bisconti, A. Giuri, R. Suhonen, T. M. Kraft, M. Ylikunnari, V. Holappa, P. Po', P. Biagini, A. Savoini, G. Marra, S. Colella and A. Rizzo, *Cell Rep. Phys. Sci.*, 2021, **2**, 100639.

68 F. Bisconti, A. Giuri, N. Vanni, S. Carallo, S. Spera, R. Marrazzo, R. Po', P. Biagini, B. Paci, A. Generosi, M. Guaragno, C. Esposito Corcione, A. Listorti, S. Colella and A. Rizzo, *Nanoscale Adv.*, 2025, **7**, 2145.

69 Y. Guo, H. S. Patanwala, B. Bognet and A. W. K. Ma, *Rapid Prototyp. J.*, 2017, **23**, 562.

70 C.-M. Hsieh, Y.-S. Liao, Y.-R. Lin, C.-P. Chen, C.-M. Tsai, E. Wei-Guang Diau and S.-C. Chuang, *RSC Adv.*, 2018, **8**, 19610.

71 B. Ding, Y. Li, S.-Y. Huang, Q.-Q. Chu, C.-X. Li, C.-J. Li and G.-J. Yang, *J. Mater. Chem. A*, 2017, **5**, 6840.

72 S. Öz, A. K. Jena, A. Kulkarni, K. Mouri, T. Yokoyama, I. Takei, F. Ünlü, S. Mathur and T. Miyasaka, *ACS Energy Lett.*, 2020, **5**, 1292.

73 A. Farooq, M. R. Khan, T. Abzieher, A. Voigt, D. C. Lupascu, U. Lemmer, B. S. Richards and U. W. Paetzold, *ACS Appl. Energy Mater.*, 2021, **4**, 3083.

74 Z. Liu, D. Liu, H. Chen, L. Ji, H. Zheng, Y. Gu, F. Wang, Z. Chen and S. Li, *Nanoscale Res. Lett.*, 2019, **14**, 304.

75 J. M. C. da Silva Filho, V. A. Ermakov and F. C. Marques, *Sci. Rep.*, 2018, **8**, 1563.

76 M. Vásquez-Montoya, J. F. Montoya, D. Ramirez and F. Jaramillo, *J. Energy Chem.*, 2021, **57**, 386.

77 S. Bae, S. J. Han, T. J. Shin and W. H. Jo, *J. Mater. Chem. A*, 2015, **3**, 23964.

78 L. Zhu, Y. Xu, P. Zhang, J. Shi, Y. Zhao, H. Zhang, J. Wu, Y. Luo, D. Li and Q. Meng, *J. Mater. Chem. A*, 2017, **5**, 20874.

79 J. Herterich, C. Baretzky, M. Unmüssig, C. Maheu, N. Glissmann, J. Gutekunst, G. Loukeris, T. Mayer, M. Kohlstädt, J. P. Hofmann and U. Würfel, *Sol. RRL*, 2022, **6**(7), 2200195.

80 S. Zhang, F. Ren, Z. Sun, X. Liu, Z. Tan, W. Liu, R. Chen, Z. Liu and W. Chen, *Small Methods*, 2024, **8**(7), 2301223.

81 T. Singh, S. Öz, A. Sasinska, R. Frohnhoven, S. Mathur and T. Miyasaka, *Adv. Funct. Mater.*, 2018, **28**(14), 1706287.

This journal is © The Royal Society of Chemistry 2025

J. Mater. Chem. A, 2025, **13**, 28200–28212 | **28211**

82 J. Haddad, B. Krogmeier, B. Klingebiel, L. Krückemeier, S. Melhem, Z. Liu, J. Hüpkes, S. Mathur and T. Kirchartz, *Adv. Mater. Interfaces*, 2020, **7**, 2000366.

83 B. Chaudhary, T. M. Koh, B. Febriansyah, A. Bruno, N. Mathews, S. G. Mhaisalkar and C. Soci, *Sci. Rep.*, 2020, **10**, 429.

84 K. Dhivyaprasath and M. Ashok, *Sol. Energy*, 2023, **255**, 89.

85 M. E. O'Kane, J. A. Smith, T. I. Alanazi, E. J. Cassella, O. Game, S. van Meurs and D. G. Lidzey, *ChemSusChem*, 2021, **14**, 2537.

86 B. Dou, L. M. Wheeler, J. A. Christians, D. T. Moore, S. P. Harvey, J. J. Berry, F. S. Barnes, S. E. Shaheen and M. F. A. M. van Hest, *ACS Energy Lett.*, 2018, **3**, 979.

87 N. Li, S. Pratap, V. Körstgens, S. Vema, L. Song, S. Liang, A. Davydok, C. Krywka and P. Müller-Buschbaum, *Nat. Commun.*, 2022, **13**, 6701.

88 D. P. McMeekin, P. Holzhey, S. O. Fürer, S. P. Harvey, L. T. Schelhas, J. M. Ball, S. Mahesh, S. Seo, N. Hawkins, J. Lu, M. B. Johnston, J. J. Berry, U. Bach and H. J. Snaith, *Nat. Mater.*, 2023, **22**, 73.

89 Y. Yuan and J. Huang, *Acc. Chem. Res.*, 2016, **49**, 286.

90 W. Tress, M. Yavari, K. Domanski, P. Yadav, B. Niesen, J. P. Correa Baena, A. Hagfeldt and M. Graetzel, *Energy Environ. Sci.*, 2018, **11**, 151.

28212 | *J. Mater. Chem. A*, 2025, **13**, 28200–28212

This journal is © The Royal Society of Chemistry 2025